

Scaling law for the onset of the surface wrinkling of multilayer tubes

Motohiro Sato,¹ Kazusa Ishigami,² Hiroyuki Kato,¹ Yoshitaka Umeno,³ and Hiroyuki Shima^{4,*}

¹*Division of Mechanical and Aerospace Engineering, Faculty of Engineering, Hokkaido University, Kita 13 Nishi 8, Sapporo 060-8628, Japan*

²*Division of Socio-Environmental Engineering, Graduate School of Engineering, Hokkaido University, N13-W8, Kita-ku, Sapporo, Hokkaido 060-8628, Japan*

³*Institute of Industrial Science, The University of Tokyo, 4-6-1 Komaba, Meguro-ku, Tokyo 153-8505, Japan*

⁴*Department of Environmental Sciences, University of Yamanashi, 4-4-37, Takeda, Kofu, Yamanashi 400-8510, Japan*

(Dated: August 11, 2020)

Surface wrinkling is an instability mode that is often observed in a wide variety of multilayer tubes under bending deformation. When the degree of applied bending exceeds a critical value, wrinkles appear at the intrados of the tube and release a large amount of in-plane strain energy stored by bending deformation. In the present work, we propose a simple theoretical model for evaluating the critical curvature and critical bending moment for the occurrence of wrinkling in multilayer tubes and apply the model to carbon nanotubes in a case study. Results indicate an inverse proportional relationship between the two critical properties, which holds true regardless of the number of layers and the size of the hollow core.

I. INTRODUCTION

Coaxially stacked tubular structures are omnipresent in nature and technology¹. Actual realizations in living matter include self-assembled microtubules in cells^{2,3}, blood vessels⁴, and lipid tubes⁵⁻⁸, whose biological functions are attributed to their multilayered tubular structures⁹⁻¹¹. In the field of nanotechnology, series of multiwalled nanotubes have been successfully synthesized; those made from carbon^{12,13}, boron nitride^{14,15}, silica¹⁶, a noble metal^{17,18}, WS₂^{19,20}, and TiO₂²¹ are only a few to mention. Furthermore, coaxial multilayered cylinders have merit in the design of macroscale composite materials in many engineering fields²²⁻²⁴.

An important benefit of coaxial multilayered tubes, compared with monolayer tubes, is the enhanced mechanical robustness of the original circular cross-section against bending. When a thin and initially straight monolayer tube is bent gradually, the tube cross-section first ovalizes²⁵ and then collapses locally by forming a sharp ridge connecting two kinks^{26,27}. These cross-sectional deformations are largely suppressed in multilayered cases. The suppression is primarily due to the steric effect; *i.e.*, inner tubes push back the inward deflection of outer tubes, thus preventing the cross-sections from severe deformation under bending. Above a threshold of bending, however, the steric effect is insufficient to suppress the deflection and another type of instability mode is likely to appear, *i.e.*, surface wrinkling. Surface wrinkling is wavelike distortion along the compressed intrados of the tubes, through which the compressed intrados is allowed to accommodate the bending-induced compressive strain. Surface wrinkling is a universal instability mode in that it has been observed in a wide variety of deformable materials with high aspect ratios, such as thick rubber cuboids²⁸, rubber scrolls²⁹, and macroscale monolayer metal tubes³⁰.

To evolve multilayered tube applications, it is important to identify the conditions under which surface wrinkling occurs; *i.e.*, we want to identify the number of tubes stacked coaxially and the degree of bending of the tube axis that result in surface wrinkling. The phenomenon is nonlinear in nature, and an exact evaluation of the conditions thus requires complicated and expensive numerical simulations, as was shown in the case of multiwalled carbon nanotubes (MWNTs). It is widely known that bending deformation strongly affects the physical properties of MWNTs³¹⁻³⁴, and intense numerical efforts have thus been made to reveal the surface morphology and energetics of wrinkled MWNTs³⁵⁻⁴³. In complementing such numerical simulations, an elastic approximation based on shell theory is an alternative simple and effective approach for obtaining the wrinkling nature.

In the present work, we propose a simple theoretical model for estimating the approximate shape and bending occurrence threshold of surface wrinkling of multilayer tubes. Using the model, we calculate the critical curvature of the tube axis and the critical bending moment for the surface wrinkling of MWNTs. The two critical properties are found to obey a simple rule, which provides an important guideline for maximum bending deflection. The applicability of the simple rule to multilayer tubes with different spatial scales, even macroscopic multilayer tubes, is discussed.

II. METHOD OF ANALYSIS

A. Elastic approximation model

Surface wrinkling has been observed for many multiwalled nanotubes made of carbon^{35,44-48}, boron nitride⁴⁹⁻⁵¹, and inorganic materials^{52,53}. In those nanomaterials, interaction between adjacent monoatomic lay-

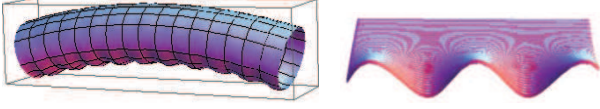


FIG. 1. Left: Diagonal view of a thick MWNT under bending; only the outmost wall is presented. A wave-shaped corrugation pattern appears on the compressed side when a bending moment above a threshold is applied. Right: Enhanced view of the corrugated intrados.

ers originates from intermolecular van der Waals (vdW) forces and is thus weak compared with strong chemical bonding¹². This anisotropy in mechanical stiffness causes surface wrinkling under bending (see Fig. 1); the flexibility of individual layers in response to out-of-plane deflection, relative to the high rigidity of the individual layers against in-plane deformation, allows the release of an appreciable amount of membrane strain energy through surface wrinkling at the expense of a slight increment in vdW energy.

Figure 2 illustrates our analytical model of MWNTs, comprising many continuum thin elastic tubes with length L . We assume that MWNTs deform with constant curvature under the application of pure bending characterized by the bending moment M . N is the number of concentric tubes while r_i is the radius of the i -th tube defined by

$$r_i = r_1 + (i - 1)d. \quad (1)$$

Here, d is the interlayer distance. The equilibrium spacing between neighboring walls is set to $d = 0.3415$ nm, in accordance with the results of previous studies⁵⁴.

B. Strain energy

The cross-sectional shape of an elastic hollow tube under pure bending is evaluated using thin-shell theory. The theory states that the total strain energy U for an N -walled tube to deform is written as the sum of three energy terms; the general form is given by⁵⁵

$$U = \sum_{i=1}^N U_{\theta}^{(i)} + \sum_{i=1}^N U_z^{(i)} + \sum_{i,j}' U_I^{(ij)}. \quad (2)$$

Here, $U_{\theta}^{(i)}$ is the strain energy associated with the circumferential displacement of a volume element in the i -th wall, $U_z^{(i)}$ is that associated with the axial displacement, and U_I accounts for the interaction between two adjacent walls. All three energy terms are functions of the curvature Γ of the deformed tube axis and the local displacement of the i -th wall represented by a set of mutually perpendicular vectors $\mathbf{u}_i, \mathbf{v}_i, \mathbf{w}_i$ (see Fig. 2). Amplitudes of the vectors, denoted by u_i, v_i, w_i , indicate the displacements of a volume element in the radial, circumferential, and axial directions, respectively. Specifically when considering the surface wrinkling of N -walled systems with

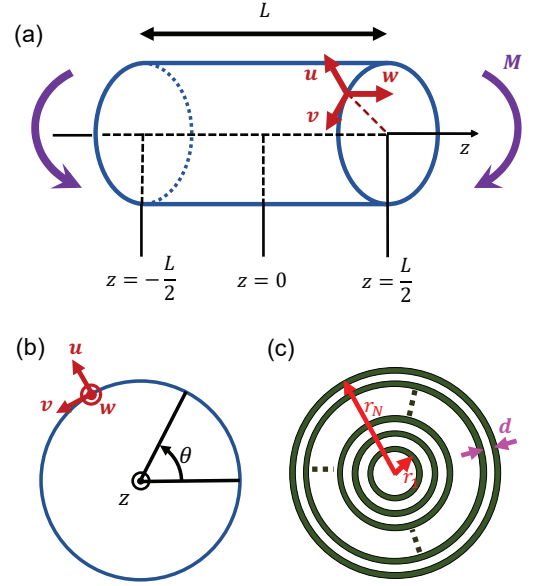


FIG. 2. (a) Continuum elastic model of an individual tube under bending. A set of three displacement vectors, $\mathbf{u}, \mathbf{v}, \mathbf{w}$, and the bending moment M are depicted. (b) Cross-sectional view of the model. (c) Definitions of the tube radius r_i ($i = 1, 2, \dots, N$) and interwall distance d .

$N \gg 1$, we are allowed to set $v_i \equiv 0$ for every i as explained later. But for the time being, we will proceed with general theory without making this assumption.

The circumferential strain energy $U_{\theta}^{(i)}$ of the i -th wall is explicitly given by

$$U_{\theta}^{(i)} = \frac{r_i}{2} \int_0^L dz \int_0^{2\pi} d\theta \left(\frac{C}{1-\nu^2} \varepsilon_{\theta}^2 + D\kappa_{\theta}^2 \right), \quad (3)$$

where

$$\varepsilon_{\theta} = \frac{u_i + \partial_{\theta} v_i}{r_i} + \frac{(\partial_{\theta} u_i - v_i)^2}{2r_i^2}, \quad \kappa_{\theta} = -\frac{\partial_{\theta}^2 u_i - \partial_{\theta} v_i}{r_i^2}. \quad (4)$$

The symbol ∂_{θ} indicates the partial derivative with respect to θ . The constant C denotes the in-plane stiffness, D the flexural rigidity, and ν the Poisson ratio of each wall. In actual calculations, we substitute $C = 345$ nN/nm, $D = 0.238$ nN·nm, and $\nu = 0.149$ by following the previous work⁵⁶ based on density functional theory.

In a similar manner, the axial strain energy $U_z^{(i)}$ is given by

$$U_z^{(i)} = \frac{r_i}{2} \int_0^L dz \int_0^{2\pi} d\theta \left(\frac{C}{1-\nu^2} \varepsilon_z^2 + D\kappa_z^2 \right), \quad (5)$$

with the definitions

$$\varepsilon_z = \partial_z w_i + \frac{(\partial_z u_i)^2}{2} + \frac{(\partial_z v_i)^2}{2}, \quad \kappa_z = \partial_z^2 u_i. \quad (6)$$

The interaction energy is defined by

$$U_I^{(ij)} = \frac{\chi_{ij}(r_i + r_j)}{4} \int_0^L dz \int_0^{2\pi} d\theta_i (u_i - u_j)^2, \quad (7)$$

where χ_{ij} is the effective spring constant per surface area, which serves as a measure of the vdW interaction strength. The explicit function form of χ_{ij} and its derivation were detailed in Ref.⁵⁷.

It is noteworthy that the values of C and D depend on the tube radius, in principle. Nevertheless, the dependencies become negligible when the tube radius exceeds 0.5 nm, above which the elastic constants of carbon nanotubes converge to those of a planar graphene sheet⁵⁶. Against this background, we consider only the nanotubes whose radii are larger than 0.5 nm, which allows us to fix the values of C and D as noted above.

C. Surface wrinkling mode analysis

To identify the bending threshold for the occurrence of surface wrinkling, we decompose the displacement of a volume element in the i -th tube as

$$\begin{aligned} u_i(z, \theta) &= u_i^*(z, \theta) + \delta u_i(z, \theta), \\ v_i(z, \theta) &= v_i^*(z, \theta) + \delta v_i(z, \theta), \\ w_i(z, \theta) &= w_i^*(z, \theta) + \delta w_i(z, \theta). \end{aligned} \quad (8)$$

The symbols marked by an asterisk are displacements in the stable mode, during which wrinkling has not yet happened such that the cross-section remains uniform along the tube axis. Those marked by δ are infinitesimal displacements just after the occurrence of the surface wrinkling mode, which are to be observed immediately after the degree of bending exceeds a critical threshold.

We make a few assumptions for the displacement components to simplify the model. First, we recall that, when considering many-walled nanotubes with $N \gg 1$, the ovalization effect observed in the stable mode can be small and negligible⁵⁵. We thus set $u_i^* = 0$ and $v_i^* = 0$ for simplicity. Second, we assume that the axial displacement in the stable mode is given by

$$w_i^* = r_i \Gamma \left(z - \frac{L}{2} \right) \sin \theta, \quad (9)$$

taking into account the elongation and shrinkage of the extrados (at $\theta = \pi/2$) and intrados ($\theta = -\pi/2$), respectively, as a result of pure bending. Third, in the wrinkling mode analysis, we ignore the contributions of δv_i and δw_i to the strain energy, because they have minor effects on the surface morphology of thick MWNTs⁵⁵. We thus focus only on the pronounced contribution of δu_i . Finally, we expand δu_i using a Fourier cosine series with respect to θ up to second order as

$$\delta u_i = \left[a_i + b_i \cos \left(\theta - \frac{\pi}{2} \right) + c_i \cos 2\theta \right] \sin \left(\frac{n\pi}{L} z \right). \quad (10)$$

In the second term in the square brackets, the phase shift of $-\pi/2$ is artificially added to achieve the situation that the amplitude of δu_i at the compressed intrados is maximized. The integer n defined in Eq. (10) indicates the number of waves on the compressed intrados.

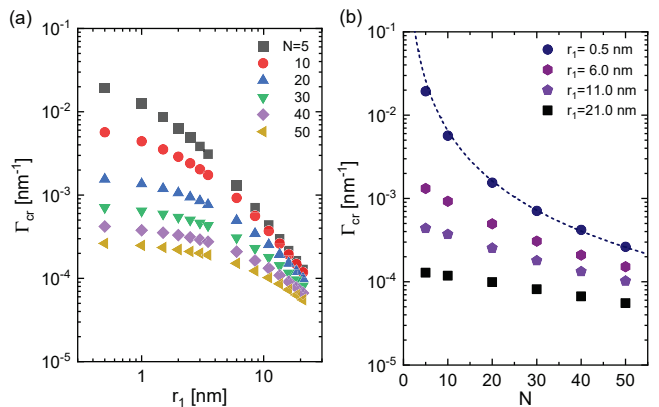


FIG. 3. (a) Critical bending curvature Γ_{cr} as a function of (a) the innermost wall radius r_1 and (b) the number of walls N . The dotted curve obeys a power law of $\Gamma_{cr} \propto N^{-2}$.

Substituting the function forms of u_i, v_i, w_i described above into Eq. (2) and rearranging the equation with respect to the order of three Fourier coefficients, a_i, b_i, c_i , we obtain the expression

$$U = U^* + \delta U(a_i, b_i, c_i) + \delta^2 U(a_i^2, b_i^2, c_i^2). \quad (11)$$

To determine the critical buckling point, we impose the stability condition that the differentiation of the second variation in strain energy, $\delta^2 U$, with respect to the Fourier expansion coefficients should be zero:

$$\frac{\partial(\delta^2 U)}{\partial a_i} = 0, \quad \frac{\partial(\delta^2 U)}{\partial b_i} = 0, \quad \frac{\partial(\delta^2 U)}{\partial c_i} = 0. \quad (12)$$

Solving Eqs. (12) under the conditions of $a_i^2 + b_i^2 + c_i^2 \neq 0$ for all i gives a series of curvature Γ as a function of n , each of which may cause surface wrinkling with wavenumber n . Among them, the minimum value of Γ corresponds to the critical curvature Γ_{cr} , which is to be observed in experiments. The critical bending moment, M_{cr} , is given by

$$M_{cr} = \pi C \Gamma_{cr} \sum_{i=1}^N (r_i)^3. \quad (13)$$

III. RESULTS

A. Critical curvature

Figure 3(a) shows the critical curvature Γ_{cr} of N -walled nanotubes as a function of r_1 . In actual calculation, the innermost tube radius r_1 is increased from 0.5 to 21.0 nm and the number of constituent walls N is varied between 5 and 50; the tube length L is fixed at 102.0 nm. In Fig. 3(a), a monotonic decrease in Γ_{cr} with increasing r_1 is observed for each value of N , indicating that an increase in the outermost tube radius r_N reduces the

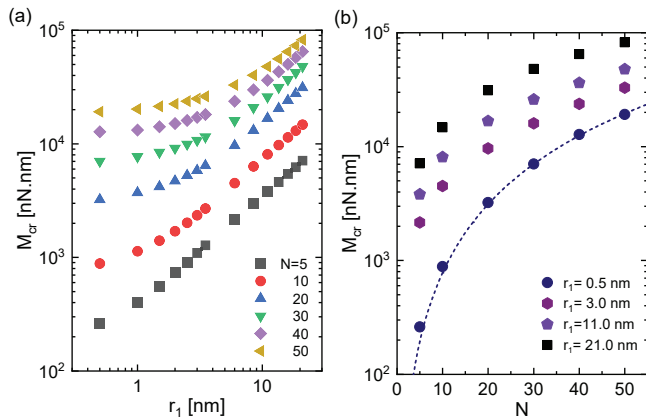


FIG. 4. (a) Critical bending moment M_{cr} as a function of (a) the innermost wall radius r_1 and (b) the number of walls N . The dotted curve obeys a power law of $M_{cr} \propto N^2$.

degree of bending that suffices for surface wrinkling to happen. For instance, the system with $r_1 = 0.5$ nm and $N = 5$ (*i.e.*, $r_N \simeq 3.4$ nm) shows wrinkling in the event of pure bending defined by $\Gamma \simeq 2 \times 10^{-2} \text{ nm}^{-1}$, which corresponds to the curvature radius of the tube axis being on the order of 100 nm, comparable to the tube length. Meanwhile, the critical curvature radius for the system with $r_1 = 21.0$ nm and $N = 5$ (*i.e.*, $r_N \simeq 16$ nm) is estimated to be $\sim 10 \mu\text{m}$, which is 100 times that in the previous case. Similar trends are found in the results for each value of N .

Figure 3(b) illustrates how Γ_{cr} depends on the number of walls N when r_1 is fixed. It follows that for a smaller r_1 , the data are well fitted by a negative power law with an exponent of -2 . Even for a larger r_1 , this power law applies if the net thickness of an N -walled tube, defined by $(N - 1)d$ or equivalently $r_N - r_1$, is larger than the innermost tube radius r_1 .

B. Critical bending moment

Figure 4(a) presents the r_1 dependence of the critical bending moment M_{cr} of N -walled nanotubes. For each value of N , M_{cr} is found to increase monotonically with increasing r_1 . The monotonic increase indicates the necessity of applying a larger bending moment for wrinkles to emerge when bending a thicker MWNT. In other words, it is a consequence of the stiffening effect against bending achieved by increasing the radius of the outermost tube.

Figure 4(b) shows rapid increases in M_{cr} with N , where the data for the small r_1 collapse onto a power law with an exponent of 2. Again, this power law holds true for the system satisfying $(N - 1)d > r_1$, in which the entire system can be considered as densely stacked multilayered tubes with a very thin cavity.

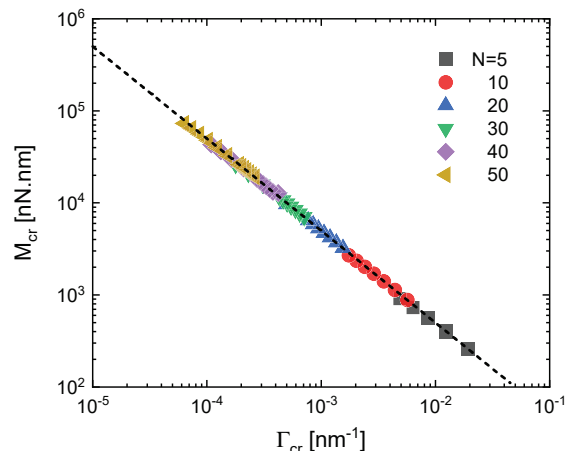


FIG. 5. Log-log plot of the M_{cr} - Γ_{cr} curve. Data collapse onto a unified power law of $M_{cr} \propto \Gamma_{cr}^{-1}$.

C. Scaling law

We demonstrate that two characteristic quantities of surface wrinkling, M_{cr} and Γ_{cr} , obey a simple scaling law under a certain condition. Figure 5 shows a log-log plot of M_{cr} and Γ_{cr} derived from systems satisfying the densely stacked criterion that $(N - 1)d > r_1$. The graph clearly shows that all data collapse onto a simple relation given by

$$M_{cr}\Gamma_{cr} = k, \quad (14)$$

with the constant $k = 5.0$ nN, as long as the criterion is satisfied. Among the data points calculated from the systems having the same number of tubes N , those located in the upper left (or lower right) are obtained from MWNTs having a small (large) r_1 .

IV. DISCUSSION

A. Scale invariance of the constant k

The following discussion derives the scaling law of Eq. (14) using an approximation theory and proves that the constant k given in Eq. (14) is scale invariant and thus dependent on neither N nor r_1 .

We first recall that the buckling behavior of *axially compressed* circular cylindrical shells has been a subject discussed for many decades in the field of structural mechanics. When a cylindrical shell with a long slender shape is compressed axially, it buckles sideways as a whole. The situation is different for a shorter cylindrical shell; *i.e.*, when a cylindrical shell with a radius R and a medium length $L \simeq R$ is compressed axially, the shell buckles locally while the cylindrical axis remains straight⁵⁸. The critical strain ε_{cr} for such local buckling

in the Lorenz limit⁵⁹ reads

$$\varepsilon_{\text{cr}} = \frac{2}{R} \sqrt{\frac{D}{C}}, \quad (15)$$

where C and D are respectively the in-plane stiffness and flexural rigidity of the shell.

We now hypothesize that Eq. (15) applies to local deformation (*i.e.*, surface wrinkling) of the compressed side of the outermost wall of a MWNT under pure *bending*. The critical strain for surface wrinkling at the compressed intrados may then be described by

$$\varepsilon_{\text{cr}}(N, r_1) = \frac{2}{r_N(N, r_1)} \sqrt{\frac{D}{C}}, \quad (16)$$

where the presence or absence of the dependence on the variables N and r_1 is explicitly shown. Considering the geometric meaning of Γ_{cr} , $\varepsilon_{\text{cr}}(N, r_1)$ should satisfy the relation

$$\varepsilon_{\text{cr}}(N, r_1) = r_N(N, r_1) \Gamma_{\text{cr}}(N, r_1). \quad (17)$$

Eliminating ε_{cr} from the two equations above, we obtain

$$\Gamma_{\text{cr}}(N, r_1) = \frac{2}{[r_N(N, r_1)]^2} \sqrt{\frac{D}{C}}, \quad (18)$$

which implies

$$\Gamma_{\text{cr}}(N, r_1) [r_N(N, r_1)]^2 = 2 \sqrt{\frac{D}{C}} = \text{const.} \quad (19)$$

It is emphasized that the constant on the right hand side, $2\sqrt{C/D}$, is independent of both N and r_1 .

As to the critical bending moment, it follows from definition that

$$M_{\text{cr}}(N, r_1) = \pi C \Gamma_{\text{cr}}(N, r_1) \sum_{i=1}^N [r_i(r_1)]^3. \quad (20)$$

When $(r_N - r_1)/r_1 > 1$ and $N \gg 1$, the sum of the cubes of r_i involved on the right-hand side of Eq. (20) can be approximately expressed by

$$\sum_{i=1}^N [r_i(r_1)]^3 \simeq \frac{[r_N(N, r_1)]^4}{4d}, \quad (21)$$

as can be derived from

$$\sum_{i=1}^N \left(\frac{r_i}{r_N} \right)^3 = \sum_{i=1}^N \left[\left(1 - \frac{Nd}{r_N} \right) + \frac{d}{r_N} i \right]^3 \simeq \frac{N}{4}, \quad (22)$$

where $r_i = r_N - (N - i)d$ has been imposed on the left-hand side.

From Eqs. (19)–(21), we have

$$M_{\text{cr}}(N, r_1) [r_N(N, r_1)]^{-2} = \frac{\pi \sqrt{CD}}{2d} = \text{const} \quad (23)$$

and

$$M_{\text{cr}}(N, r_1) \Gamma_{\text{cr}}(N, r_1) = \frac{\pi D}{d}. \quad (24)$$

We eventually conclude that the constant k given in Eq. (14) is approximately equal to $\pi D/d$, which involves neither N nor r_1 as expected.

An intriguing physical consequence deduced from Eq. (24) is that the product of M_{cr} and Γ_{cr} is determined only by D/d ; *i.e.*, the characteristic force that is required to transform a thin elastic plate with flexural rigidity D into a cylinder with radius of curvature d . This result implies that if elastic membranes having flexural rigidity D are coaxially stacked with the same membrane spacing d , the resulting multilayer tube follows the scaling law of Eq. (14), regardless of the number of membranes stacked.

B. Occurrence conditions for the scaling law

We have demonstrated that, for the scaling law of Eq. (14) to occur, many hollow tubes must be densely stacked around a common tubular axis; this condition is mathematically expressed by $(N - 1)d > r_1$. Under the densely stacked condition, the presence of many inner tubes suppresses inward deformation of outer tubes so that the original circular cross-section remains kept during bending until the surface wrinkling takes place. Particularly in the case of MWNTs' model, the effective spring constant, χ_{ij} in Eq. (7), needs to be larger than a threshold to prevent the inward penetration of the outer tube. But we should note that the effective spring constant is not a unique way to represent the interlayer coupling; any kind of interaction will result in the scaling law as long as it suppresses the cross-sectional deformation under the condition of $(N - 1)d > r_1$. In multilayered rubber tubes²⁹, for instance, adjacent layers do not exert forces on each other when they are separated; the steric exclusion does work only when they are in contact with each other. Still in the latter case, what is necessary for the scaling law realization will be the densely stacked condition, similar to the case of MWNTs.

Another necessary condition for the scaling law to occur is that the system should be long and slender enough so that the shell theory can apply to the analysis of buckling behaviors under bending. It was argued that, given an elastic hollow cylinder with length L and diameter $2r$, its slenderness should be quantified not by the aspect ratio $L/(2r)$ but the dimensionless parameter.^{60,61}

$$\Omega = \sqrt{\frac{L^2 h}{r^3}}, \quad (25)$$

with h being the wall thickness of the hollow cylinder. When Ω is larger than 0.5 or a bit more, the cylinder can be considered slender enough so that the shell theory applies⁶¹; as a consequence, the surface wrinkling occurs in the N -walled systems with $N \gg 1$. Given this

criterion, most of the MWNTs we have dealt with can be classified to slender systems, provided that the individual wall thickness be $h \sim 0.34$ nm. Nevertheless, the above-mentioned is only a guideline and not a strict criteria for the slenderness of MWNTs, because the wall is made out of a monoatomic-thick layer and thus the notion of a wall thickness be elusive.

C. Possible means to verify the scaling law

The remaining important question is to verify that the theoretically predicted scaling law holds in real MWNTs. A possible way for verifying it by experiments is to directly observe the bending-induced deformation process using an electron microscope. In fact, many in-situ nanomechanical experiments have been conducted so far on the bending process of MWNTs^{35,44–48}; a cantilevered nanotube was deflected inside an electron microscope, by which the tube geometry under bending and the loading imposed were accurately measured. Using the technique, it will be possible to measure the critical bending moment and critical curvature of a given MWNT, from which we can verify the applicability of the scaling law we have derived. The same applies to nanoscale multiwalled tubes other than those made of carbon, such as boron nitride nanotubes⁵¹.

Large-scale numerical simulation is also a powerful tool for verifying the scaling law in multiwalled nanotube systems. For example, it has been demonstrated that MD calculations can be used to simulate the surface wrinkling of 10-walled nanotubes composed of hundreds of thousands of carbon atoms⁶². The coarse-grained method can also be used to analyze MWNTs containing by far more atoms^{36,40}. In addition, the finite element method was proven to be useful for reproduction of the surface wrinkling of MWNTs obtained by electron micrograph images⁶³. We believe that these computational approaches would enable us to verify the scaling law for various kinds of multiwalled nanotubes.

We conjecture that the scaling law of Eq. (14) holds true even for macroscopic multilayer tubular systems, considering the generality of our theoretical approach. Indeed, the surface wrinkling was observed when bending a rubber multilayer tube that is made by rolling up a thin palm-sized rubber sheet²⁹. Similar wrinkling mode will be observable in Kapton tubes⁶⁴ and gel cylinders⁶⁵

if they are stacked coaxially to realize multilayered tubular systems. In such the macroscopic tubular systems, the measurement of the critical bending moment and the critical curvature is easier than in the nanotube systems. They thus allow to test whether the scaling law applies not only to nanoscopic but also macroscopic systems. Theoretical analysis on the surface wrinkling of a long rubber block⁶⁶ may also be a clue to address the problem.

Furthermore, the wrinkling mode is expected when the hollow cavity of a thin-walled monolayer tube is filled with an elastic medium with high bulk modulus (*e.g.*, a liquid or powder), because almost no cross-sectional ovalization occurs even when a bending stress is applied. The same is true for thick monolayer tubes where the radius of the hollow cavity is sufficiently smaller than the tube radius. It is therefore interesting to scrutinize the generality of the scaling law for the surface wrinkling of various multilayer tubes that cover a wide range of spatial scales; the results may give us a common rule for the mechanics of multilayer tubes under bending loading.

V. CONCLUSION

We constructed a simple theoretical model to describe the surface wrinkle phenomenon that occurs in MWNTs with pure bending. Using this model, we derived the inverse proportional law of the critical curvature Γ_{cr} and critical bending moment M_{cr} and gained the theoretical insight that the proportionality factor has a scale-free property independent of the outer (r_N) and inner (r_1) tube radii and the number of graphene walls N . It is expected that our theoretical model is basically applicable to a broad class of multilayer tube structures, and not limited to MWNTs, by imposing appropriate material parameters and interlayer energy expressions specific to the systems to be considered. We hope that the results presented will contribute to the development of applied technologies for multilayer tubes.

ACKNOWLEDGMENTS

This work was supported by JSPS KAKENHI Grant Numbers 18H03818, 18K18801, 19H02020, 19H05359, and 19K03766.

* hshima@yamanashi.ac.jp; (Correspondence author)

¹ T. Shimizu, M. Masuda, and H. Minamikawa, Chem. Rev. **105**, 1401 (2005).

² D. Sept and F. C. MacKintosh, Phys. Rev. Lett. **104**, 018101 (2010).

³ G. J. Brouhard and L. M. Rice, Nat. Rev. Mol. Cell Biol. **19**, 451 (2018).

⁴ J. M. Silva, C. A. Custódio, R. L. Reis, and J. ao F. Mano, ACS Biomater. Sci. Eng. **2**, 2304 (2016).

⁵ Y. Zhao, N. Mahajan, R. Lu, and J. Fang, Proc. Natl. Acad. Sci. USA **102**, 7438 (2005).

⁶ Y. Zhao, L. An, and J. Fang, Phys. Rev. E **80**, 021911 (2009).

⁷ Y. Sekine, K. Abe, A. Shimizu, Y. Sasaki, S. ichi Sawada, and K. Akiyoshi, RSC Advances **2**, 2682 (2012).

- ⁸ S. E. Ghellab and X. Han, Chem. Phys. Lett. **706**, 515 (2018).
- ⁹ H.-S. Shen, Phys. Lett. A **374**, 4030 (2010).
- ¹⁰ M. Taj and J. Q. Zhang, Biochem. Biophys. Res. Commun. **424**, 89 (2012).
- ¹¹ Y. Gao and L. An, Physica E **42**, 2406 (2010).
- ¹² H. Shima and M. Sato, *Elastic and Plastic Deformation of Carbon Nanotubes* (Pan Stanford Publishing, Singapore, 2012).
- ¹³ H. Shima, Materials **5**, 47 (2012).
- ¹⁴ C. Zhi, Y. Bando, C. Tang, and D. Golberg, Mater. Sci. Eng. R **70**, 92 (2010).
- ¹⁵ M. Zheng, C. Ke, I.-T. Bae, C. Park, M. W. Smith, and K. Jordan, Nanotechnology **23**, 095703 (2012).
- ¹⁶ T. Delclos, C. Aimé, E. Pouget, A. Brizard, I. Huc, M.-H. Delville, and R. Oda, Nano Lett. **8**, 1929 (2008).
- ¹⁷ P. Gao, C. Zhan, and M. Liu, Langmuir **22**, 775 (2006).
- ¹⁸ J. Zhu, J.-J. Li, and J.-W. Zhao, J. Nanopart. Res. **15**, 1721 (2013).
- ¹⁹ I. Kaplan-Ashiri, S. R. Cohen, K. Gartsman, V. Ivanovskaya, T. Heine, G. Seifert, I. Wiesel, H. D. Wagner, and R. Tenne, Proc. Natl. Acad. Sci. U.S.A. **103**, 523 (2006).
- ²⁰ E. Kalfon-Cohen, O. Goldbart, R. Schreiber, S. R. Cohen, D. Barlam, T. Lorenz, A. Enyashin, and G. Seifert, J. Vac. Sci. Technol. B **29**, 021009 (2011).
- ²¹ J. Qiu, F. Zhuge, X. Li, X. Gao, X. Gan, L. Li, B. Weng, Z. Shi, and Y.-H. Hwang, J. Mater. Chem. **22**, 3549 (2012).
- ²² M. Sato and M. H. Patel, J. Marine Sci. Technol. **12**, 251 (2007).
- ²³ M. Sato, M. Patel, and F. Trarieux, Str. Eng. Mech. **30**, 263 (2008).
- ²⁴ T. Ozbakkaloglu, Eng. Str. **51**, 188 (2013).
- ²⁵ L. G. Brazier, Proc. Roy. Soc. Lond. Math. Phys. A **116**, 104 (1927).
- ²⁶ S. Kyriakides and T. G. Ju, Int. J. Solids Struct. **29**, 1117 (1992).
- ²⁷ A. E. Lobkovsky, Phys. Rev. E **53**, 3750 (1996).
- ²⁸ A. N. Gent and I. S. Cho, Rubber Chem. Technol. **72**, 253 (1996).
- ²⁹ L. Mahadevan, J. Bico, and G. McKinley, Europhys. Lett. **65**, 323 (2004).
- ³⁰ H. Yang and Y. Lin, J. Mater. Process. Technol. **152**, 363 (2004).
- ³¹ A. Rochefort, P. Avouris, F. Lesage, and D. R. Salahub, Phys. Rev. B **60**, 13824 (1999).
- ³² A. A. Farajian, B. I. Yakobson, H. Mizuseki, and Y. Kawazoe, Phys. Rev. B **67**, 205423 (2003).
- ³³ J. Ma, Y. Ni, S. Volz, and T. Dumitrică, Phys. Rev. Appl. **3**, 024014 (2015).
- ³⁴ H. M. Ouakad and H. M. Sedighi, Int. J. Non-Linear Mech. **87**, 97 (2016).
- ³⁵ P. Poncharal, Z. L. Wang, D. Ugarte, and W. A. de Heer, Science **283**, 1513 (1999).
- ³⁶ M. Arroyo and T. Belytschko, Phys. Rev. Lett **91**, 215505 (2003).
- ³⁷ T. Chang and J. Hou, J. Appl. Phys. **100**, 114327 (2006).
- ³⁸ X. Y. Li, W. Yang, and B. Liu, Phys. Rev. Lett **98**, 205502 (2007).
- ³⁹ X. Huang, J. Zou, and S. L. Zhang, Appl. Phys. Lett. **93**, 031915 (2008).
- ⁴⁰ M. Arroyo and I. Arias, J. Mech. Phys. Solids **56**, 1224 (2008).
- ⁴¹ I. Nikiforov, D. B. Zhang, R. D. James, and T. Dumitrică, Appl. Phys. Lett. **96**, 123107 (2010).
- ⁴² C. G. Wang, Y. P. Liu, J. Al-Ghalith, T. Dumitrică, M. K. Wadee, and H. F. Tan, Carbon **102**, 224 (2016).
- ⁴³ J. Zare and A. Shateri, Physica E **90**, 67 (2017).
- ⁴⁴ T. Kuzumaki, T. Hayashi, H. Ichinose, K. Miyazawa, K. Ito, and Y. Ishida, Phil. Mag. A **77**, 1461 (1998).
- ⁴⁵ O. Lourie, D. M. Cox, and H. D. Wagner, Phys. Rev. Lett. **81**, 1638 (1998).
- ⁴⁶ C. Bower, R. Rosen, L. Jin, J. Han, and O. Zhou, Appl. Phys. Lett. **74**, 3317 (1999).
- ⁴⁷ H. Jackman, P. Krakhmalev, and K. Svensson, Appl. Phys. Lett. **104** (2014).
- ⁴⁸ H. Jackman, P. Krakhmalev, and K. Svensson, J. Appl. Phys. **117**, 084318 (2015).
- ⁴⁹ D. Golberg, P. M. F. J. Costa, O. Lourie, M. Mitome, X. Bai, K. Kurashima, C. Zhi, C. Tang, and Y. Bando, Nano Lett. **7**, 2146 (2007).
- ⁵⁰ Y. Huang, J. Lin, J. Zou, M.-S. Wang, K. Faerstein, C. Tang, Y. Bando, and D. Golberg, Nanoscale **5**, 4840 (2013).
- ⁵¹ H. M. Ghassemi, C. H. Lee, Y. K. Yap, and R. S. Yassar, Nanotechnology **22**, 115702 (2011).
- ⁵² M. S. Wang, I. Kaplan-Ashiri, X. L. Wei, R. Rosentsveig, H. D. Wagner, R. Tenne, and L. M. Peng, Nano. Res. **1**, 22 (2008).
- ⁵³ E. W. Bucholz and S. B. Sinnott, J. Appl. Phys. **112**, 123510 (2012).
- ⁵⁴ L. A. Girifalco, M. Hodak, and R. S. Lee, Phys. Rev. B **62**, 13104 (2000).
- ⁵⁵ H. Shima, M. Sato, and S. J. Park, Adv. Condens. Mat. Phys. **2014**, 923896 (2014).
- ⁵⁶ K. N. Kudin, G. E. Scuseria, and B. I. Yakobson, Phys. Rev. B **64**, 235406 (2001).
- ⁵⁷ H. Shima, S. Ghosh, M. Arroyo, K. Iiboshi, and M. Sato, Comp. Mater. Sci. **52**, 90 (2012).
- ⁵⁸ J. Feliciano, C. Tang, Y. Zhang, and C. Chen, J. Appl. Phys. **109**, 084323 (2011).
- ⁵⁹ R. Lorenz, Phys. Z. **12**, 241 (1911).
- ⁶⁰ H. Shima, M. Sato, and A. Inoue, Phys. Rev. E **93**, 022406 (2016).
- ⁶¹ J. Wang, O. K. Fajuyitan, M. A. Orabi, J. M. Rotter, and A. J. Sadowski, J. Construct. Steel Res. **166**, 105920 (2020).
- ⁶² X. Li, W. Yang, and B. Liu, Phys. Rev. Lett. **98**, 205502 (2007).
- ⁶³ A. Pantano, D. M. Parks, and M. C. Boyce, J. Mech. Phys. Solids **52**, 789 (2004).
- ⁶⁴ Q. X. Ji, C. G. Wang, and H. F. Tan, Int. J. Mech. Sci. **126**, 1 (2017).
- ⁶⁵ A. Ghatak and A. L. Das, Phys. Rev. Lett. **99**, 076101 (2007).
- ⁶⁶ N. Padukka and J. Hill, Math. Mech. Solids **19**, 308 (2012).